

Soft Matter

Accepted Manuscript



This is an *Accepted Manuscript*, which has been through the Royal Society of Chemistry peer review process and has been accepted for publication.

Accepted Manuscripts are published online shortly after acceptance, before technical editing, formatting and proof reading. Using this free service, authors can make their results available to the community, in citable form, before we publish the edited article. We will replace this *Accepted Manuscript* with the edited and formatted *Advance Article* as soon as it is available.

You can find more information about *Accepted Manuscripts* in the [Information for Authors](#).

Please note that technical editing may introduce minor changes to the text and/or graphics, which may alter content. The journal's standard [Terms & Conditions](#) and the [Ethical guidelines](#) still apply. In no event shall the Royal Society of Chemistry be held responsible for any errors or omissions in this *Accepted Manuscript* or any consequences arising from the use of any information it contains.

Cite this: DOI: 10.1039/xxxxxxxxxx

Investigation of PDMS based bi-layer elasticity via interpretation of apparent Young's modulus

Baptiste Sarrazin^{†*}, Rémy Brossard^{†*}, Patrick Guenoun[†], Florent Malloggi[†]Received Date
Accepted Date

DOI: 10.1039/xxxxxxxxxx

www.rsc.org/journalname

As the need of new methods for the investigation of thin films on various kinds of substrates becomes greater, a novel approach based on AFM nanoindentation is explored. Substrates of polydimethylsiloxane (PDMS) coated by a layer of hard material are probed with an AFM tip in order to obtain the force profile as a function of the indentation. The equivalent elasticity of those composite systems is interpreted using a new numerical approach, the Coated Half-Space Indentation Model of Elastic Response (CHIMER), in order to extract the thicknesses of the upper layer. Two kinds of coating are investigated. First, chitosan films of known thicknesses between 30 and 200 nm were probed in order to test the model. A second type of samples is produced by oxygen plasma oxidation of the PDMS substrate, which results in the growth of a relatively homogeneous oxide layer. The local nature of this protocol enables measurements at long oxidation time, where the apparition of cracks prevents other kinds of measurements.

1 Introduction

With the rise of micro and nanotechnology, thin films on a substrate are used increasingly in technological applications. In particular, the controlled alteration of surfaces has been extensively studied as a promising tool for the development of new systems. One famous example is the surface oxidation of polydimethylsiloxane (PDMS), which is used to change the wetting and adhesion properties of the surface¹ and to bond covalently the material to another one, as in soft lithography techniques². The chemical state of such an altered system has been studied by many methods, such as contact angle measurement or X-ray spectroscopy^{3–5}. Yet, although the mechanical properties of these submicrometer thin films are of utmost importance – for their stability and direct use in microfabrication⁶ – the dimensional and mechanical characterization is difficult due to the influence of the substrate^{7,8}.

In the case of a soft substrate coated or covered with a harder surface, wrinkling technique has been implemented to investigate the layer properties like the thickness^{9–11}. If a mechanically expanded soft material is coated by a harder material, wrinkles will form at the surface when the stress is released as the lower layer shrinks. The wavelength of these wrinkles is directly related to the ratio of the elastic moduli of the materials and its measurement enables one to deduce the thickness of the top layer. A

first issue of the method is the soundness of the perfect bilayer assumption on a quite large scale (compared to the wavelength of the wrinkles). In the case of oxidized PDMS for example, the apparition of surface cracks prevents the use of that method for plasma exposure times larger than ten minutes at 30 W⁹. A second problem is that the wrinkles method cannot be used as a preliminary to another experiment. Indeed, the samples have to be dedicated to these measurements as they will keep the wrinkles stigmata.

An alternative non destructive method for the nanoscale investigation of homogeneous materials is AFM nanoindentation¹² often coupled to the use of Hertz model¹³. In particular, AFM nanoindentation has been demonstrated to be a valid approach in the case of thin homogeneous polymer films^{14–16}. During the last twenty years, it has been also used to study materials properties for non-planar geometries and various non-homogeneous systems such as microbubbles^{17–20}, microcapsules^{21–23}, hollow colloidal particles^{24,25}, nanotubes²⁶, thin virus shell²⁷, polymer brushes^{28,29} and even living cells^{30–32}. Nevertheless, the composite nature of the materials, either due to their shapes or the multiplicity of their compounds, complicates the interpretation of these measurements. In that respect, computed elasticities determined from force-indentation curves are only effective values, that need to be carefully interpreted.

The case of hard coating of a soft substrates has been mainly study in the fields of flexible electronics³³ and biological system like for cells³⁴. However those approach rely only on the existence of an initial regime, when the surface is probed alone, and a final regime, when the bulk is probed alone. Thus, every pieces

* B. Sarrazin and R. Brossard contributed equally to this work

† Interdisciplinary Laboratory on Nanoscale and Supramolecular Organizations, NIMBE, CEA, CNRS, Université Paris-Saclay, CEA Saclay 91191 Gif sur Yvette Cedex, France - corresponding author: florent.malloggi@cea.fr

of information contained in the transition are lost. Hence, an easy way to interpret this apparent modulus remains the critical challenge for the AFM nanoindentation reliability.

On theoretical grounds, finite element analysis has proved itself to be valid for the investigation of bilayers, coated materials or membranes, but this method can be awkward and demanding to implement for experimental purpose^{35,36}. However, the particular case of a thin layer material on a thick substrate indented by an axisymmetric indenter is simple enough to be theoretically approached and compared to experiments. Based on the work of Li and Chou³⁷, Perriot and Barthel³⁸ proposed an exact integral formulation of the problem which can be semi-analytically solved. In this paper, we reformulated this model as a function of experimental parameters and call the result Coated Half-space Indentation Model of Elastic Response (CHIMER). This model provides a relation between the geometrical parameters of the system (tip geometry and film thickness), indentation depth and elastic moduli of the materials. One can in principle extract the hard layer thickness from an indentation profile. The advantages of the method are that dedicated samples are not needed and that measurements are easy and repeatable after a proper calibration is performed. Moreover the relevant scale of the measurement is the nanometer which remains often a limit for the classic imaging methods. Despite all those attractive features, this model has never been tested experimentally to our knowledge.

In the present work, we demonstrate how to interpret the effective elastic moduli from force-indentation curves and make use of that technique for the study of two different bi-layer samples. The common thread within both systems is a PDMS thick substrate ($\approx 10\mu\text{m}$, Young's modulus $E_{PDMS} = 2.6\text{ MPa}$ and Poisson's ratio $\nu = 0.5$) which is topped with a harder and thin layer. First, chitosan films of known thicknesses between 30 and 200 nm were probed in order to test and qualify the model. Chitosan^{39,40} is a linear polysaccharide which is used for biomedical application. Elasticity values of chitosan span a relatively large range in literature depending on the solvent used for film preparation and the drying conditions used for making bulk samples. In order to match our experimental conditions, microindentation has been performed on bulk sample. The chitosan films were made by spin-coating parameters and the thicknesses were checked afterward by AFM. As a result, the analysis of equivalent elasticities thanks to CHIMER is shown to retrieve the chitosan thicknesses with a satisfying precision. In a second part, the properties of plasma oxidized PDMS (Young's modulus 1 to 100 GPa and Poisson's ratio $\nu \approx 0.3$)^{9,10} have been investigated by the same CHIMER approach. In particular, the evolution of the thickness of the oxide layer upon long exposure times (above ten minutes at 30W) has been probed. The thickness of the oxidized layer is shown to evolve as a power law of plasma exposure time. This result expands previous studies which showed a slower evolution of the layer, hinting at a hardening of the upper material.

2 Theoretical considerations

2.1 AFM nanoindentation of bilayered sample

When performing AFM nanoindentation, an AFM cantilever is used as a force probe, deflecting itself by interaction with the surface and indenting the sample if the latter is soft enough. Typically, AFM nanoindentation provides deflection (D) vs. displacement (z) curves. Indentation (δ) is calculated from equation (1):

$$\delta = |z - z_0| - |D - D_0| \quad (1)$$

where z and D are the piezo-displacement and the cantilever deflection respectively and z_0 and D_0 are the piezo-displacement and the cantilever deflection at the position where the tip-surface contact occurs, respectively. The loading force F is determined from the Hookean equation (2) :

$$F = k(D - D_0) \quad (2)$$

where k is the spring constant of the AFM cantilever. On homogeneous materials and in absence of adhesion, Hertz model – which describes the purely elastic deformation of two spherical bodies in contact – is commonly used to interpret the elastic modulus E (Young's modulus in the case of compressive experiment) from the force-indentation curve. Flat-sphere Hertz contact model is expressed as follow:

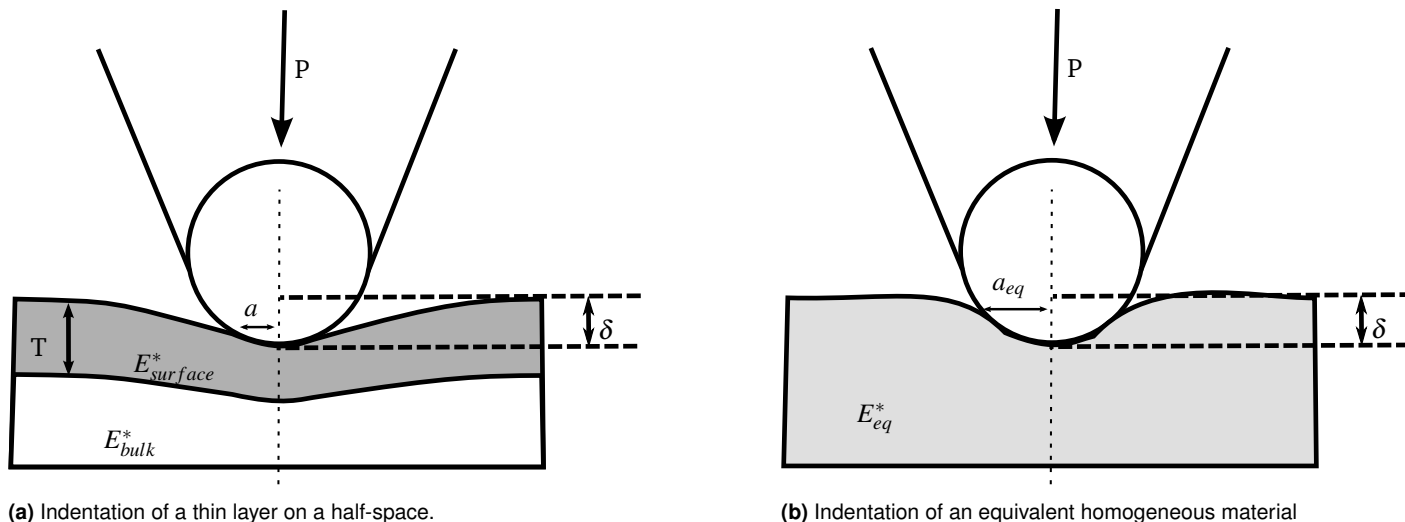
$$F = \frac{4}{3}\sqrt{RE^*}\delta^{3/2} \quad (3)$$

$$E^* = \frac{E}{1 - \nu^2} \quad (4)$$

where R is the radius of the tip, F is the applied force, δ is the indentation depth, ν is the Poisson ratio of the sample and E^* is the reduced elastic modulus. Usually, the equation 3 to the power 2/3 is used and the contact point δ_0 (origin of δ) is shifted to improve the fit. This approach is mathematically equivalent to a fit of both the modulus and the contact point. In this study, ν is set to 0.5 for the 1:10 cross linked PDMS⁴¹ and 0.3 for the chitosan (glassy polymer). Concerning the oxidized PDMS layer, Poisson ratio is assumed to be 0.3 that is in between 0.5 (ν_{PDMS}) and 0.18 (ν_{SiO_2})⁴².

2.2 Coated Half-space Indentation Model of Elastic Response (CHIMER)

We consider the case of a semi-infinite substrate covered by a layer of thickness T of different elastic moduli. The force measured as a function of mechanical displacement of a material probed by a well-defined tip can be interpreted in term of an equivalent modulus E_{eq}^* i.e. the modulus measured for a given indentation δ with Hertz formula (eq. 3) for the system considered as homogeneous as in figure 1. The three dimensional nature of such system allows tangential dissipation of the stress in the two materials, so that if the top layer is infinitely thick all the effort is released in it and the equivalent modulus amounts to the reduced modulus $E_{surface}^*$ of the top layer. On the opposite, if it is extremely thin, most of the effort is dissipated in the underlying material and the equivalent modulus is the reduced modulus



(a) Indentation of a thin layer on a half-space.

(b) Indentation of an equivalent homogeneous material

Fig. 1 Indentation of the real layered system and its equivalent homogeneous system. The latter is defined by an equivalent modulus and a new contact radius, as the compliance of the surface is different. The latter radius follows the standard Hertzian relation $a_{eq} = \sqrt{\delta R}$

E_{bulk}^* of the bulk underlying material. Hence, the measurement of an effective modulus is in fact an evaluation of the ratio δ/T , i.e. an interpolation between the two bulk moduli. Those values can be calculated thanks to a numerical model proposed by Perriot and Barthel³⁸ which provides E_{eq}^* and $\Delta = \delta/\delta_{Hertz}$ (with $\delta_{Hertz} = a^2/R$) as a function of a/T . This model is referred to as a Coated Half-space Indentation Model of Elastic Response (CHIMER).

The basis of this model is then to introduce a weight function Φ defined as:

$$E_{eq}^* = E_{bulk}^* + \Phi(E_{surface}^* - E_{bulk}^*) \quad (5)$$

With the hypothesis of Hertz model (normal displacement field), Li and Chou³⁷ solved the punctual elastic response function of a coated half-space system. However, due to the mixed boundary conditions, the solution could not be integrated for a real tip geometry. Perriot and Barthel solved this integration problem by introducing auxiliary fields, turning the problem into an integral system of equations that can be solved numerically. This model reproduces the transition of the equivalent modulus as the ratio between the contact radius a and surface thickness T evolves (see figure 2) for different tip shapes (e.g. spherical, conic or flat punch). This is a practical problem as when performing AFM nanoindentation, the natural *experimental* parameter is the indentation δ and not the real contact radius a . More over the Hertzian relation between the *physical* parameter a and *experimental* parameter δ ($a_{Hertz} = \sqrt{\delta R}$) does not hold anymore. In order to make this method practically relevant, the relation between the correction factor to the contact radius a/a_{Hertz} and the ratio of indentation over thickness δ/T is required. This can simply be obtained by numerically inverting the $\delta_{CHIMER}(a)$ relation provided by CHIMER, as displayed in the inset of figure 2. In practice, for computational efficiency, we adjust a so that $\delta_{CHIMER}(a)$ converges to a target $\delta_{experimental}$. Ultimately, we obtain a relation between the effective modulus and the indentation

depth. If the surface modulus is known, the layer thickness can be obtained with the knowledge of E_{eq}^* , the tip radius R , and the corresponding indentation depth δ .

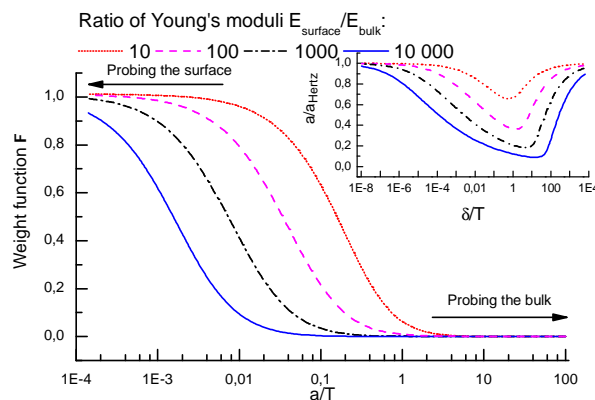


Fig. 2 Main plot: Simulated transition of the weight function Φ for different modulus mismatches using a spherical probe. Inset: Computed correction to the Hertzian relation $a_{Hertz} = \sqrt{\delta R}$. The original relation provided by Perriot et al.³⁸ is δ as a function of a and was inverted for practical purposes.

3 Experimental Section

3.1 Atomic Force Microscopy

We used an AFM Dimension V (Digital Instruments / Veeco-Bruker, Santa Barbara, CA, USA) mounted with an optical microscope. All force measurements are performed in air. Particular attention is paid to cantilever calibration and tip geometry measurement as described in the following section. Three different AFM cantilevers have been used in order to probe mechanical properties from 1 MPa to 10 GPa: DNP (Bruker, $0.06-0.7 \text{ N.m}^{-1}$), FESPA (Bruker, $1-5 \text{ N.m}^{-1}$) and B1-NCHR (Nanotools, 42 N.m^{-1}). For indentation use, the tip can be viewed as spherical of radius

precisely characterized using deconvolution algorithms and found to be in between 10 to 20 nm.

3.2 Sample Preparation

Silicon wafer substrates are cleaned by UV-Ozone, plasma and acid technique⁴³ to get reproducible wetting and surface state. Sylgard polydimethylsiloxane is mixed with the furnished cross-linker with a ratio 10:1 and spin-coated on the substrate at 3000 RPM for one minute with an acceleration on 500 RPM.s⁻¹. The samples are then placed on a hot plate at 150 °C for 15 minutes to ensure a complete cross-linking of the material.

Oxidized PDMS samples are prepared in a *Harrick's* plasma cleaner. Oxygen is supplied to the chamber where the pressure is regulated by the equilibrium between the oxygen entrance flow rate (monitored with a microvalve) and a fixed outflow. The pressure is set to 4.10⁻¹ mbar and the plasma is powered on at 29.6 W for a measured time.

Chitosan from Sigma Aldrich is dissolved in chlorhydric acid (pH = 1). The dissolution process is slow and can be accelerated by extended sonication. In order to prepare chitosan on PDMS samples, those are exposed to plasma for one minute to make the surface hydrophilic. The chitosan solution can then be spin-coated on the substrate for one minute with an acceleration on 500 RPM.s⁻¹ and adapted rotational speeds. The samples are then dried for one hour at 80 °C on a hot plate.

3.3 Thickness control

The thickness of the substrate PDMS layer has been measured to be 10 μm ± 2 μm with an optical interferometer. As the surface of oxidized PDMS resembles that of silica⁴⁴, the thickness of a spin-coated layer of chitosan is not expected to change much if the substrate is clean silicon or oxidized PDMS. Hence, chitosan was spin-coated on clean silicon wafers with relevant parameters. A scratch was formed on the film with a razor blade and the thickness of the layer was measured by AFM.

3.4 Calibration of the Cantilever Spring Constant k

Measurement of mechanical response of the cantilever to thermal noise is used to compute spring constant (Lorentzian fit of the frequency spectrum). The cantilever stiffness calibration procedure can be describe as follow: force curve on hard surface is performed and the slope of approaching curve is measured to know the sensitivity of the cantilever. Then thermal tune is made far from the surface and the frequency spectrum is fitted around the peak which is at the resonant frequency.

3.5 AFM Tip Geometry

Indirect measurement using deconvolution algorithm has been used to determine the radii of AFM tips. This procedure can be considered as reverse imaging. Indeed, it consists in a characterization surface imaging with the tip of interest. Blind deconvolution algorithm⁴⁵ is applied to this picture and allows to get back to the tip shape. Deconvolution is computed using Gwyddion software (David Nečas and Petr Klapetek, Department of Nanotech-

nology, Czech Metrology Institute). Characterization surface used for blind deconvolution of our tips consists of pyramidal hard sharp nanostructures (PA series from Mikromasch, NanoAndMore GmbH).

4 Results and Discussion

4.1 Curve interpretation

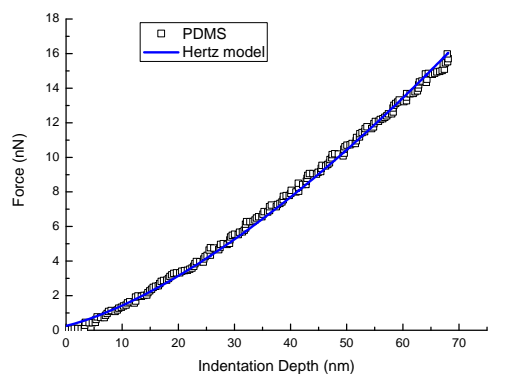
As the effective modulus drops with the indentation depth, the force is expected to deviate from the $\delta^{3/2}$ behavior predicted on an homogeneous sample. This was observed for hard coatings on a soft substrate for example by Kaushik et al.⁴⁶ where two limiting Hertz-like behaviors are observed corresponding successively to the probing of the hard coating and then to the soft substrate. In our case, this is illustrated in figure 3. The indentation of an homogeneous sample displays a $F \propto E^* \delta^{3/2}$ behavior while a coated sample is closer to a linear behavior. This dependency can be interpreted by using CHIMER simulation. Indeed, we can provide typical values for Young's moduli and coating thickness of our samples to the model. As displayed in figure 4, the relation obtained predicts that the effective modulus decreases as the inverse square-root of indentation. Hence, because $F \propto E_{eq}^*(\delta) \delta^{3/2}$, a linear behavior is expected.

The Tabor parameter μ of the PDMS is about 40 to 5000⁴⁷ because of the adhesion extent, giving the Johnson-Kendall-Roberts model⁴⁸ as the more appropriate. By contrast, for bilayers the Young's modulus is increased, meaning that larger forces must be applied. Hence, one can believe that such materials behave in a way such as adhesion can be treated as a perturbation by the linearized Hertz model. A first attempt to interpret the experimental force curves is then to perform a linearized Hertz fit where the force curve is fitted to a Hertz function with the elasticity and the contact point as fit parameters on a limited delta range [0.1 δ_{max} ; 0.7 δ_{max}]. Because of the use of the contact point as a fit parameter, the adhesive regime as less influence on the fit result on the indentation range. Hence, a smaller indentation is needed to reach the elastic regime without noticeable influence of the adhesive regime. The use of this limited range enables one, within the CHIMER framework, to interpret the fitted elasticity \bar{E}^* as an average of the bilayer equivalent elasticity $E_{eq}^*(\delta)$ on the fit range. Such a fit is shown in Figures 3b and 3c.

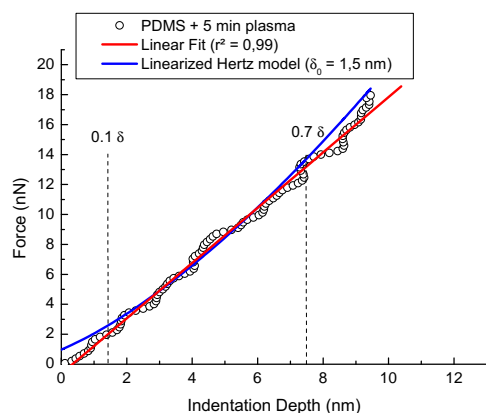
Within the CHIMER framework and in order to interpret the fitted moduli, the corresponding average indentations $\bar{\delta}$ has to be properly calculated. The linearized Hertz model is a least square linear regression of the linear relation obtained with eq. 3 to the power 2/3. The residual to be minimized is :

$$\Pi = \left\langle \left(F_i^{2/3} - \left(\frac{4}{3} \sqrt{R} \right)^{2/3} \bar{E}^*{}^{2/3} \delta \right)^2 \right\rangle \quad (6)$$

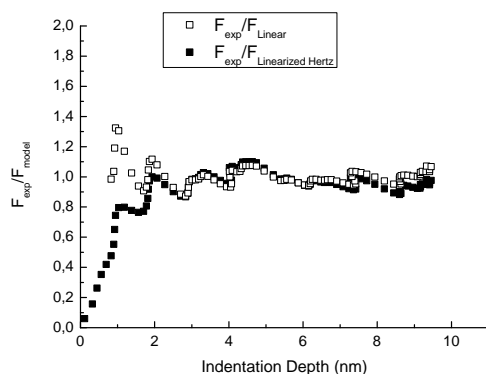
where $\langle \cdot \rangle$ is the average on the fit range. Minimizing this expression for experimental δ_i uniformly distributed and $E_{eq}^* \propto \delta^{-1/2}$, we obtain:



(a) Homogeneous PDMS



(b) Oxidized PDMS (5 min plasma exposure)



(c) Fit quality of the heterogeneous system force curve.

Fig. 3 Force-indentation curves on homogeneous and bilayered samples. In the case of the heterogeneous sample, the linearized Hertz model (fitted between $0.1 \delta_{max}$ and $0.7 \delta_{max}$) is compared to the linear fit.

$$\begin{aligned} \bar{E}^* &= E_{eq}^* \left(\left[\left(\frac{\langle \delta^2 \rangle}{\langle \delta^{5/3} \rangle} \right)^3 \right] \right) = E_{eq}^*(\bar{\delta}) \\ \bar{\delta} &= \left[\left(\frac{\langle \delta^2 \rangle}{\langle \delta^{5/3} \rangle} \right)^3 \right] \end{aligned} \quad (7)$$

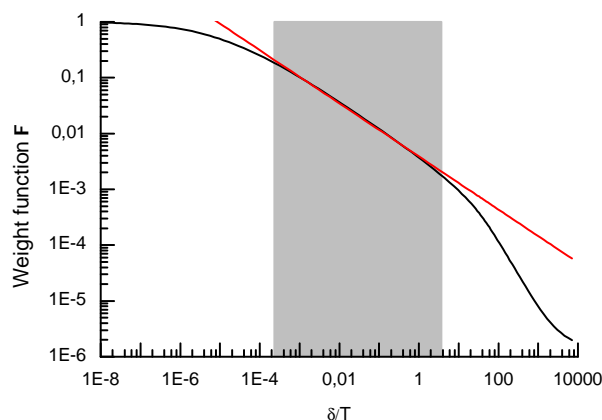


Fig. 4 Power dependence of E_{eq}^* as a function of δ . Simulated evolution of the apparent modulus with a top layer thickness $T = 12 \text{ nm}$ and radius of tip $R = 20 \text{ nm}$. All measurements were performed in the gray zone where the fitted power (slope) is -0.48 .

In order to avoid problems of adhesion and plasticity and to ensure a good fit quality (see Fig 3c.), the fit range is taken between $0.1 \delta_{max}$ and $0.7 \delta_{max}$, so that the average indentation depth is $\bar{\delta} = 0.5 \delta_{max}$. One has to note that as the contact point is also fitted in that model, the shift in origin has to be taken into account when calculating $\bar{\delta}$. Using CHIMER, the couple of values $E_{eq}^*, \bar{\delta}$ can be finally used to recover the thickness of the top layer.

As shown in figures 3b and 3c, a linear fit of the force curve is of an even better quality, as expected. This can be interpreted by taking variations of E_{eq}^* directly into account, which leads to the modified Hertz equation:

$$F = S\delta \text{ with } S = \frac{4}{3} \sqrt{R\delta} E_{eq}^* \quad (8)$$

where S is now a constant in δ . The S value can be used with CHIMER to obtain the value of the thickness of the top layer. This method is all the more attractive that there is no need of calculating an equivalent indentation. However, one has to note that this model is completely contact point independent. We will elaborate on this aspect later.

4.2 Chitosan-coated PDMS elasticity

To test the models, chitosan films are spin-coated on PDMS thick samples. The thicknesses of chitosan films are previously measured on silicon wafers as a reference. It has to be noted that the surface of PDMS shortly exposed to plasma is chemically close to that of glass or silicon⁴⁴, so that the thickness of chitosan films shall only depend of the spin coating parameters. Microindentation experiments are performed on thick chitosan film which is dried on a glass slide and bulk elastic modulus $E_{surface}$ of chitosan is found to be $3.0 \pm 0.1 \text{ GPa}$. AFM nanoindentation is then performed on chitosan-PDMS samples for different capping thicknesses. Multiple force-displacement curves are displayed in figure 5.

Both approaches detailed in the previous paragraph are imple-

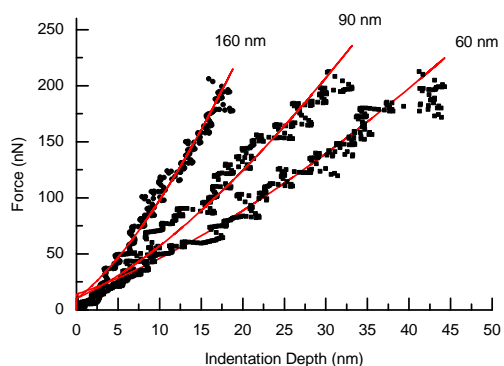


Fig. 5 Multiple force-displacement curves obtained on chitosan-coated PDMS. The solid lines are the linearized Hertzian fit realized on each curve between 10% and 70%

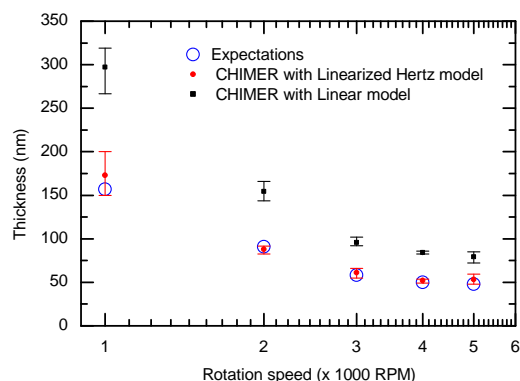


Fig. 6 Expected and calculated thicknesses of a chitosan layer on PDMS. Expected values (blue circles) are previously measured on silicon wafers. CHIMER is used to calculate thicknesses from measured apparent modulus using linearized Hertz model with indentation $0.5 \delta_{max}$ (red circles) and linear model which does not require indentation (black squares).

mented and displayed on figure 6 along with the expectations. The linearized Hertz approach calculations exhibit an excellent agreement with the expected thicknesses, giving a good confidence in the CHIMER algorithm. Although providing the qualitative correct tendency, the linear relation interpretation leads on the contrary to an overestimation of approximately 70% of the thicknesses. The differences between the models are summed up in figure 7.

On homogeneous materials, linearized Hertz model fits both the elastic modulus and the contact point, thus compensating experimental effects like adhesion. When indenting a composite material, those parameters become functions of indentation. In particular the relevant contact point (the fit-relevant origin of indentation) is only a virtual value which is not related to the actual physical contact point. When performing linearized Hertz fit on a narrow range of indentation, we obtain an average elastic modu-

lus \bar{E}^* and an average of the virtual instantaneous contact point $\bar{\delta}_0$. The linear model takes the variations of $E_{eq}^*(\delta)$ into account, but this model is contact point independent. More precisely, it assumes the contact point to be the same for each δ and well-defined. In our opinion, the failure of the linear model is a strong hint that in order to adapt a standard contact model to a composite system, both the mechanical properties and contact point must evolve during indentation (See figure 7) in order to take into account effects such as adhesion or long range forces. In the particular case of adhesion, as the contact area grows slowly with indentation, the range of indentation on which this effect holds could be much larger than on homogeneous materials. For instance, if a first-order development of the contact point with indentation holds $\delta_0^{eq}(\delta) \approx C + \alpha\delta$, the slope X is biased and becomes $X = S(1 - \frac{3}{2}\alpha)$ where S is the slope of equation 8. We plan to elaborate on such a better model in a next publication.

Homogeneous

Linearized Hertz
 $F \propto E^*(\delta - \delta_0)^{3/2}$

Bilayer

Linearized Hertz
 $F \propto \bar{E}^*(\delta - \bar{\delta}_0)^{3/2}$

Linear Model
 $F \propto E_{eq}^*(\delta)\delta^{3/2}$

Hypothetic Model

$F \propto E_{eq}^*(\delta)(\delta - \delta_0^{eq}(\delta))^{3/2}$

Fig. 7 Different routes for the conversion of the Hertzian contact model on homogeneous material for a use on composite materials indentation interpretation.

4.3 Plasma oxidized PDMS elasticity

The linearized Hertz method was used to determine the thickness of an oxidized layer of PDMS for plasma exposure time between 30 s and 90 min at 29.6 W. On figure 8 are displayed the result with a surface modulus of 1.5 GPa as found in literature⁹. The values of thickness at short time matches well values previously found in literature with wrinkling methods^{9,10}. However, although Bayley and coll.¹⁰ predicted a logarithmic progression of the thickness as a function of dose (or time at fixed power), at long time exposure the oxidized layer thickness exhibits a power law $T \propto t^{0.63}$. Apparent modulus larger than 1.5 GPa were found for exposure larger than 160 kJ which corresponds to 80 minutes of exposition (not displayed on figure 8). Thus, an increase of the surface modulus is suspected to occur. In particular, a second slower reaction could take place, generating another harder layer. This conjecture is supported by SEM pictures of a slice of PDMS previously oxidized for a very long time (data not shown). However, deeper investigation are required to support this assertion which are beyond the scope of this article.

5 Conclusion

AFM nanoindentation experiments were performed on PDMS soft substrates covered by two kinds of hard materials: chitosan and PDMS oxide. The so-called apparent measured modulus of these composite samples can be interpreted using a new semi-analytical

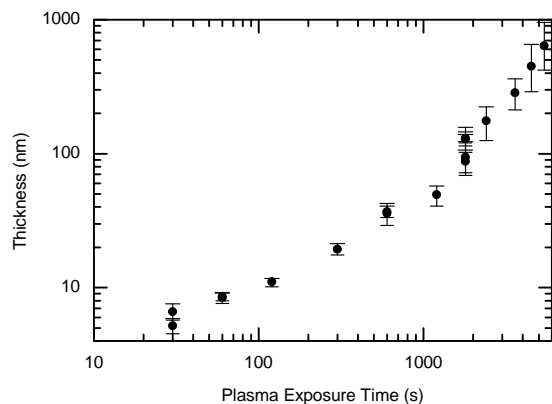


Fig. 8 Thickness of oxidized PDMS films using CHIMER.

approach called CHIMER. Two different methods have been used to obtain the equivalent elasticities which are then interpreted into CHIMER.

The chitosan layer thickness is measured by other means, so that the relevance of the models can be put at test. A very good agreement between measured and expected thicknesses is found with the linearized Hertz method. On the other hand, the linear model displays an overestimation of approximately 70% of the thicknesses. This systematic bias can be imputed to the contact point independence of this method. This mismatch of the linear model through CHIMER may be an interesting field of investigation, especially concerning the necessity to depict a virtual contact point during multilayer indentation experiments. In the oxidized PDMS case, the thicknesses are unknown and the nanoscale feature of this method is used to measure the oxide layer thickness at longer time scale than possible with other methods. The counterintuitive increase of the growth speed hints at a hardening of the surface material, that is suspected to take origin in the growth of a second harder layer.

AFM nanoindentation is a very tempting route for the investigation of the properties of thin films or coatings. However, the influence of the substrate is a major problem that is practically hard to avoid. The CHIMER approach is a potentially viable option as it can decorrelate the contribution of the layer from that of the substrate. For the first time, this model has been practically tested. Although some aspects of the methods remains to be clarified, we believe its great predictive potential has been proven.

Acknowledgement

This work was supported by the French National Research Agency, Grant n° ANR-13-IS09-0002, the RTRA Triangle de la Physique (Université Paris-Saclay) and the University Versailles Saint Quentin en Yvelines. The authors would like to thanks E. Barthel from the SIMM laboratory (UMR 7615, ESPCI, Paris, France) for his help to understand and use the CHIMER model. L. Pauchard (FAST laboratory (UMR 7608, Université Paris-Sud, Orsay, France), is acknowledged for his help in microindentation

experiment of bulk chitosan.

References

- 1 D. Bodas and C. Khan-Malek, *Sensors and Actuators B: Chemical*, 2007, **123**, 368–373.
- 2 Y. Xia and G. M. Whitesides, *Angewandte Chemie International Edition*, 1998, **37**, 550–575.
- 3 B. Schnyder, T. Lippert, R. Kötz, A. Wokaun, V.-M. Graubner and O. Nuyken, *Surface Science*, 2003, **532-535**, 1067–1071.
- 4 H. Hillborg, J. Ankner, U. Gedde, G. Smith, H. Yasuda and K. Wikström, *Polymer*, 2000, **41**, 6851–6863.
- 5 M. Morra, E. Occhiello, R. Marola, F. Garbassi, P. Humphrey and D. Johnson, *Journal of Colloid and Interface Science*, 1990, **137**, 11–24.
- 6 L. P. Chia Gómez, P. Bollgruen, A. I. Egunov, D. Mager, F. Malloggi, J. G. Korvink and V. A. Luchnikov, *Lab on a Chip*, 2013, **13**, 3827.
- 7 S. Chen, L. Liu and T. Wang, *Surface and Coatings Technology*, 2005, **191**, 25–32.
- 8 R. Saha and W. D. Nix, *Acta Materialia*, 2002, **50**, 23–38.
- 9 S. Béfhay, P. Lipnik, T. Pardoën, C. Nascimento, B. Patris, P. Bertrand and S. Yunus, *Langmuir*, 2010, **26**, 3372–3375.
- 10 F. A. Bayley, J. L. Liao, P. N. Stavrinou, A. Chiche and J. T. Cabral, *Soft Matter*, 2014, **10**, 1155.
- 11 B. A. Glatz, M. Tebbe, B. Kaoui, R. Aichele, C. Kuttner, A. E. Schedl, H.-W. Schmidt, W. Zimmermann and A. Fery, *Soft Matter*, 2015, **11**, 3332–3339.
- 12 H.-J. Butt, B. Cappella and M. Kappl, *Surface Science Reports*, 2005, **59**, 1–152.
- 13 H. R. Hertz, *Ueber die Berührung elastischer Koerper (On Contact Between Elastic Bodies)*, 1895, vol. 1.
- 14 J. Domke and M. Radmacher, *Langmuir*, 1998, **14**, 3320–3325.
- 15 P. A. O'Connell, *Science*, 2005, **307**, 1760–1763.
- 16 B. Du, O. K. C. Tsui, Q. Zhang and T. He, *Langmuir*, 2001, **17**, 3286–3291.
- 17 E. Buchner Santos, J. K. Morris, E. Glynos, V. Sboros and V. Koutsos, *Langmuir*, 2012, **28**, 5753–5760.
- 18 R. H. Abou-Saleh, S. A. Peyman, K. Critchley, S. D. Evans and N. H. Thomson, *Langmuir*, 2013, **29**, 4096–4103.
- 19 M. Poehlmann, D. Grishenkov, S. V. V. N. Kothapalli, J. Härmann, H. Hebert, A. Philipp, R. Hoeller, M. Seuss, C. Kuttner, S. Margheritelli, G. Paradossi and A. Fery, *Soft Matter*, 2014, **10**, 214.
- 20 C. A. Grant, J. E. McKendry and S. D. Evans, *Soft Matter*, 2012, **8**, 1321.
- 21 M. Ghorbanzadeh Ahangari, A. Fereidoon, M. Jahanshahi and N. Sharifi, *Composites Part B: Engineering*, 2014, **56**, 450–455.
- 22 C. de Loubens, J. Deschamps, M. Georgelin, A. Charrier, F. Edwards-Levy and M. Leonetti, *Soft Matter*, 2014, **10**, 4561.
- 23 C. Ye, I. Drachuk, R. Calabrese, H. Dai, D. L. Kaplan and V. V. Tsukruk, *Langmuir*, 2012, **28**, 12235–12244.
- 24 C. Zoldesi, I. Ivanovska, C. Quilliet, G. Wuite and A. Imhof, *Physical Review E*, 2008, **78**, year.

- 25 J. Yin, M. Retsch, J.-H. Lee, E. L. Thomas and M. C. Boyce, *Langmuir*, 2011, **27**, 10492–10500.
- 26 E. P. S. Tan and C. T. Lim, *Applied Physics Letters*, 2005, **87**, 123106.
- 27 M. Gibbons and W. Klug, *Physical Review E*, 2007, **75**, year.
- 28 X. Sui, Q. Chen, M. A. Hempenius and G. J. Vancso, *Small*, 2011, **7**, 1440–1447.
- 29 Z. Zhang, A. J. Morse, S. P. Armes, A. L. Lewis, M. Geoghegan and G. J. Leggett, *Langmuir*, 2013, **29**, 10684–10692.
- 30 M. Horimizu, T. Kawase, T. Tanaka, K. Okuda, M. Nagata, D. M. Burns and H. Yoshie, *Micron*, 2013, **48**, 1–10.
- 31 P. Carl and H. Schillers, *Pflügers Archiv - European Journal of Physiology*, 2008, **457**, 551–559.
- 32 D. Vella, A. Ajdari, A. Vaziri and A. Boudaoud, *Journal of The Royal Society Interface*, 2011, **9**, 448–455.
- 33 F. Cavallo, D. S. Grierson, K. T. Turner and M. G. Lagally, *ACS Nano*, 2011, **5**, 5400–5407.
- 34 M. R. Bonilla, J. R. Stokes, M. J. Gidley and G. E. Yakubov, *Soft Matter*, 2015, **11**, 1281–1292.
- 35 S. Liu, H. Huang and Y. Gu, *Thin Solid Films*, 2012, **526**, 183–190.
- 36 C. Zhang, M. Zhao, Y. Liu and B. Wang, *Journal of Materials Research*, 2013, **28**, 2570–2576.
- 37 J. Li and T.-W. Chou, *International Journal of Solids and Structures*, 1997, **34**, 4463–4478.
- 38 A. Perriot and E. Barthel, *Journal of Material Research*, 2004, 600–608.
- 39 A. Martínez-Camacho, M. Cortez-Rocha, J. Ezquerra-Brauer, A. Graciano-Verdugo, F. Rodríguez-Félix, M. Castillo-Ortega, M. Yépiz-Gómez and M. Plascencia-Jatomea, *Carbohydrate Polymers*, 2010, **82**, 305 – 315.
- 40 T. Nishino, R. Matsui and K. Nakamae, *Journal of Polymer Science Part B: Polymer Physics*, 1999, **37**, 1191–1196.
- 41 R. H. Pritchard, P. Lava, D. Debruyne and E. M. Terentjev, *Soft Matter*, 2013, **9**, 6037.
- 42 R. Limbach, B. P. Rodrigues and L. Wondraczek, *Journal of Non-Crystalline Solids*, 2014, **404**, 124–134.
- 43 W. Kern, *Journal of the Electrochemical Society*, 1990, **137**, 1887–1892.
- 44 H. Hillborg, J. Ankner, U. W. Gedde, G. Smith, H. Yasuda and K. Wikström, *Polymer*, 2000, **41**, 6851–6863.
- 45 J. Villarrubia, *Surface Science*, 1994, **321**, 287–300.
- 46 G. Kaushik, A. Fuhrmann, A. Cammarato and A. Engler, *Biophysical Journal*, 2011, **101**, 2629–2637.
- 47 Y. Cao, D. Yang and W. Soboyejoy, *Journal of Materials Research*, 2005, **20**, 2004–2011.
- 48 K. L. Johnson, K. Kendall and A. D. Roberts, *Proceedings of the Royal Society A: Mathematical, Physical and Engineering Sciences*, 1971, **324**, 301–313.